

Optimal Modifications of Gear Tooth Surfaces

Vilmos Simon

(Proceedings of the 3rd International Conference on Power Transmission 2009. October 1–2, 2009, Chalkidiki, Greece.)

Management Summary

In this paper a new method for the introduction of optimal modifications into gear tooth surfaces—based on the optimal corrections of the profile and diameter of the head cutter, and optimal variation of machine tool settings for pinion and gear finishing—is presented. The goal of these tooth modifications is the achievement of a more favorable load distribution and reduced transmission error. The method is applied to face milled and face hobbled hypoid gears.

Corresponding computer programs are developed. By using these programs, the optimal head cutter geometry and the optimal machine tool settings for pinion and gear tooth processing are determined. The influence of tooth errors and misalignments of the mating members on load distribution and transmission error is investigated. The obtained results show that the influence of tooth errors and misalignments on gear performances is significantly reduced by the introduction of optimal tooth modifications.

Introduction

Conjugated spur, helical, spiral bevel, hypoid and worm gears are theoretically in line contact. In order to decrease the sensitivity of the gear pair to errors in tooth surfaces and to the mutual position of the mating members, carefully chosen modifications are usually introduced into the teeth of one or both members. Over the years, much research has been directed towards the optimization of design and manufacture of different types of gears. Some of the related references are for:

- Spur and helical gears (Refs. 1–3)
- Spiral bevel and hypoid gears (Refs. 4–27)
- Cylindrical worm gears (Refs. 28–35)
- Double-enveloping worm gears (Refs. 36–40)

As a result of these modifications, the gear pair becomes

“mismatched,” and point contact of the meshed tooth surfaces appears instead of line contact. In practice, these modifications are usually introduced by applying the appropriate machine tool setting for pinion and gear manufacture, or by the optimization of the tool geometry.

The method for the determination of optimal tooth modifications—based on minimized tooth contact pressure and transmission error—is presented in the example of face milled and face hobbled hypoid gears.

Theoretical Background

The major differences between the face milling and face hobbing process are:

- In face hobbing, a timed continuous indexing is provided, while in face-milling, the indexing is intermittently provided after cutting each tooth side or slot.
- The lengthwise tooth curve of face milled hypoid gears is a circular arc with a curvature radius equal to the cutter radius, while the lengthwise tooth curve of face hobbled gears is an epicycloid that is kinematically generated by the indexing motion.
- Face hobbing gear design uses the uniform tooth depth system while face milling gear design uses the tapered tooth depth system; i.e.—the pinion is the driving member. The convex side of the gear tooth and the mating concave side of the pinion tooth are the drive sides.

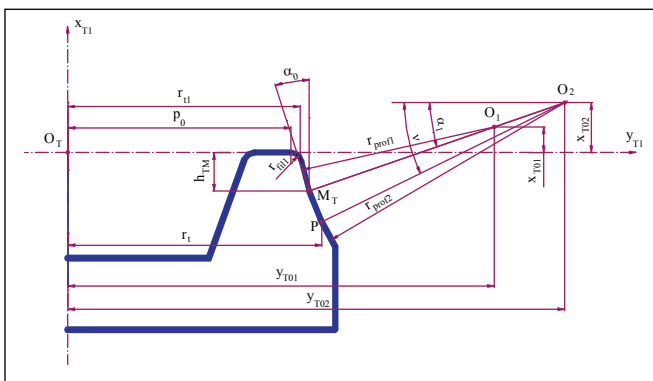


Figure 1—Bi-circular tool profile for pinion tooth finishing.

The Generation of Tooth Surfaces in Face Milled Hypoid Gears

A Gleason-type hypoid gear pair—with generated pinion and non-generated gear—is treated. The optimal tooth modifications are introduced into the pinion tooth surface by using a cutter with bi-circular profile (Fig. 1), optimal tool diameter

and appropriate machine tool settings.

The tool surface, with bi-circular profile and for the generation of the driving side of pinion teeth, is in the coordinate system Kr_1 (attached to tool T_1), defined by the following equation (and Fig. 1):

continued

Nomenclature

c, c_i	=	Sliding base setting, mm	$\Delta\phi_2^{(d)}$	=	Dynamic angular displacement of the driven gear member, arc second
d	=	Basic machine center to back increment setting for gear finishing, mm	$\Delta\phi_2^{(k)}$	=	Kinematic angular displacement of the driven gear member, arc second
e	=	Basic radial setting, mm	δ	=	Basic swivel angle setting for pinion finishing, deg
f, f_i	=	Basic machine center setting, mm	ε_h	=	Angular misalignment of pinion axis, deg
g, g_i	=	Basic offset setting, mm	ϕ_1, ϕ_2	=	Rotation angles of the pinion and gear, respectively, in mesh, deg
h	=	Basic horizontal setting for gear finishing, mm	ϕ_{10}, ϕ_{20}	=	Initial rotation angles of the pinion and gear, respectively, in mesh, deg
h_d	=	Distance from tilt center to machine plane, mm	γ_p, γ_0	=	Initial setting angle of head cutter axis, deg
h_{TM}	=	Position of cutter radii's connection point, mm	γ_1	=	Machine root setting angle for pinion finishing, deg
i_c	=	Indexing ratio	γ_2	=	Machine root angle setting for gear finishing, deg
i_g, i_{gi}	=	Velocity ratios in the kinematic scheme of the machine tool for the generation of pinion and gear tooth surfaces	η_i	=	Initial setting angle of head cutter, deg
N_b	=	Number of head cutter's blade groups	ν	=	Parameter of circular cutting edge, deg
N_c	=	Number of teeth of the imaginary generating crown gear	κ	=	Tilt angle of cutter spindle with respect to cradle rotation angle, deg
N_w	=	Number of teeth of the workpiece	μ	=	Swivel angle of cutter tilt, deg
N_1, N_2	=	Number of pinion and gear teeth	$\omega^{(c)}$	=	Angular velocity of the imaginary generating crown gear, deg
p_{max}	=	Maximum tooth contact pressure, N/cm ²	$\omega^{(r)}$	=	Angular velocity of the tool in pinion teeth generation, sec ⁻¹
r_{profi}	=	Radius of circular tool profile, mm	$\omega^{(T)}$	=	Angular velocity of the head cutter, sec ⁻¹
r_{r1}	=	Pinion finishing cutter radius, mm	$\omega^{(w)}$	=	Angular velocity of the workpiece, sec ⁻¹
r_{r2}	=	Gear finishing cutter radius, mm	θ	=	Tool surface variable, mm
s	=	Tooth thickness, mm	ρ_c	=	Radius of the rolling circle of the imaginary generating crown gear, mm
u, t	=	Tool surface variables, mm	ρ_t	=	Radius of the rolling circle of the head cutter, mm
v	=	Basic vertical setting for gear finishing, mm	ξ	=	Tool surface variable, mm
x_{epi}, z_{epi}	=	Coordinates of the center of the circular blade profile, mm	ξ_i	=	Offset angle of cutter blade, deg
x_{TOP}, y_{TOi}	=	Coordinates of the center of circular arc tool profile, mm	ψ	=	Cradle rotation angle, deg
z_{eM}	=	Position of blade profile radii's connection point, mm	ψ_i	=	Rotation angles of the pinion and the gear in the generation of tooth flanks, deg
α	=	Profile angle of the straight-lined cutting edge, deg	ψ_c	=	Rotation angle of the imaginary generating crown gear in its generation, deg
α_1	=	Pinion finishing tool profile angle, deg	ψ_{ci}	=	Rotation angle of the imaginary generating crown gear in pinion gear tooth generation, deg
α_2	=	Gear finishing tool profile angle, deg	ψ_t	=	Rotation angle of head cutter, deg
β	=	Basic tilt angle setting for pinion finishing, deg			
β_F	=	Load distribution factor			
$\Delta\phi_2$	=	Angular displacement of the driven gear member, arc second			
$\Delta\phi_{2s}$	=	Angular displacement of the driven gear member due to edge contact, arc second			

$$\vec{r}_{T1}^{(T1)}(v, \theta) = \begin{bmatrix} x_{T0i} - r_{\text{profi}} \cdot \sin v \\ (y_{T0i} - r_{\text{profi}} \cdot \cos v) \cdot \cos \theta \\ (y_{T0i} - r_{\text{profi}} \cdot \cos v) \cdot \sin \theta \\ 1 \end{bmatrix}$$

where: $i = 1, 2$ —for pinion and gear, respectively.

In the case of straight-sided profile (Fig. 2), the equation of tool surface is as follows:

$$\vec{r}_{T1}^{(T1)}(u, \theta) = \begin{bmatrix} -u \\ (r_{t1} + u \cdot \text{tg} \alpha_1) \cdot \cos \theta \\ (r_{t1} + u \cdot \text{tg} \alpha_1) \cdot \sin \theta \\ 1 \end{bmatrix}$$

The generated tooth surface of the pinion (Fig. 2) is defined by the system of equations:

$$\begin{aligned} \vec{r}_1^{(1)} &= \mathbf{M}_{p4} \cdot \mathbf{M}_{p3} \cdot \mathbf{M}_{p2} \cdot \mathbf{M}_{p1} \cdot \vec{r}_{T1}^{(T1)} \\ \vec{v}_0^{(T1,1)} \cdot \vec{e}_0^{(T1)} &= 0 \end{aligned}$$

where: $\vec{v}_0^{(T1,1)}$ is the relative velocity vector of the tool T_1 to the pinion, and $\vec{e}_0^{(T1)}$ is the unit normal vector of the tool surface.

On the basis of Figure 2 and Equations 1 and 2, for the relative velocity vector and for the unit normal vector of the tool surface, it follows that:

$$\vec{v}_0^{(T1,1)} = \omega^{(T)} \cdot \begin{bmatrix} i_g \cdot (z_0^{(T1)} + g) \cdot \cos \gamma_1 \\ z_0^{(T1)} - i_g \cdot (z_0^{(T1)} + g) \cdot \sin \gamma_1 \\ i_g \cdot [y_0^{(T1)} \cdot \sin \gamma_1 - (x_0^{(T1)} - c) \cdot \cos \gamma_1] - y_0^{(T1)} \end{bmatrix}$$

$$\vec{e}_0^{(T1)} = \mathbf{M}_{p2} \cdot \mathbf{M}_{p1} \cdot \vec{e}_{T1}^{(T1)} = \mathbf{M}_{p2} \cdot \mathbf{M}_{p1} \begin{bmatrix} \sin q \\ \cos q \cdot \cos \theta \\ \cos q \cdot \sin \theta \\ 0 \end{bmatrix}$$

where: $q = \alpha_1$ is in the case of straight-sided tool profile; $q = v$ in the case of bi-circular profile and:

$$\vec{r}_0^{(T1)} = \mathbf{M}_{p2} \cdot \mathbf{M}_{p1} \cdot \vec{r}_{T1}^{(T1)}$$

Matrices $\mathbf{M}_{p1} - \mathbf{M}_{p4}$ provide the coordinate transformations from the coordinate system K_{T1} (attached to the tool) into the system K_j (attached to the pinion). The coordinate transformations are defined by the following equations (Fig. 2):

$$\vec{r}_{T0} = \mathbf{M}_{p1} \cdot \vec{r}_{T1} = \begin{bmatrix} \cos \beta & -\sin \beta & 0 & 0 \\ \cos \delta \cdot \sin \beta & \cos \delta \cdot \cos \beta & -\sin \delta & 0 \\ \sin \delta \cdot \sin \beta & \sin \delta \cdot \cos \beta & \cos \delta & 0 \\ 0 & 0 & 0 & 1 \end{bmatrix} \cdot \vec{r}_{T1}$$

$$\vec{r}_0 = \mathbf{M}_{p2} \cdot \vec{r}_{T0} = \begin{bmatrix} 1 & 0 & 0 & 0 \\ 0 & \sin \psi & -\cos \psi & e \cdot \cos \psi \\ 0 & \cos \psi & \sin \psi & -e \cdot \sin \psi \\ 0 & 0 & 0 & 1 \end{bmatrix} \cdot \vec{r}_{T0}$$

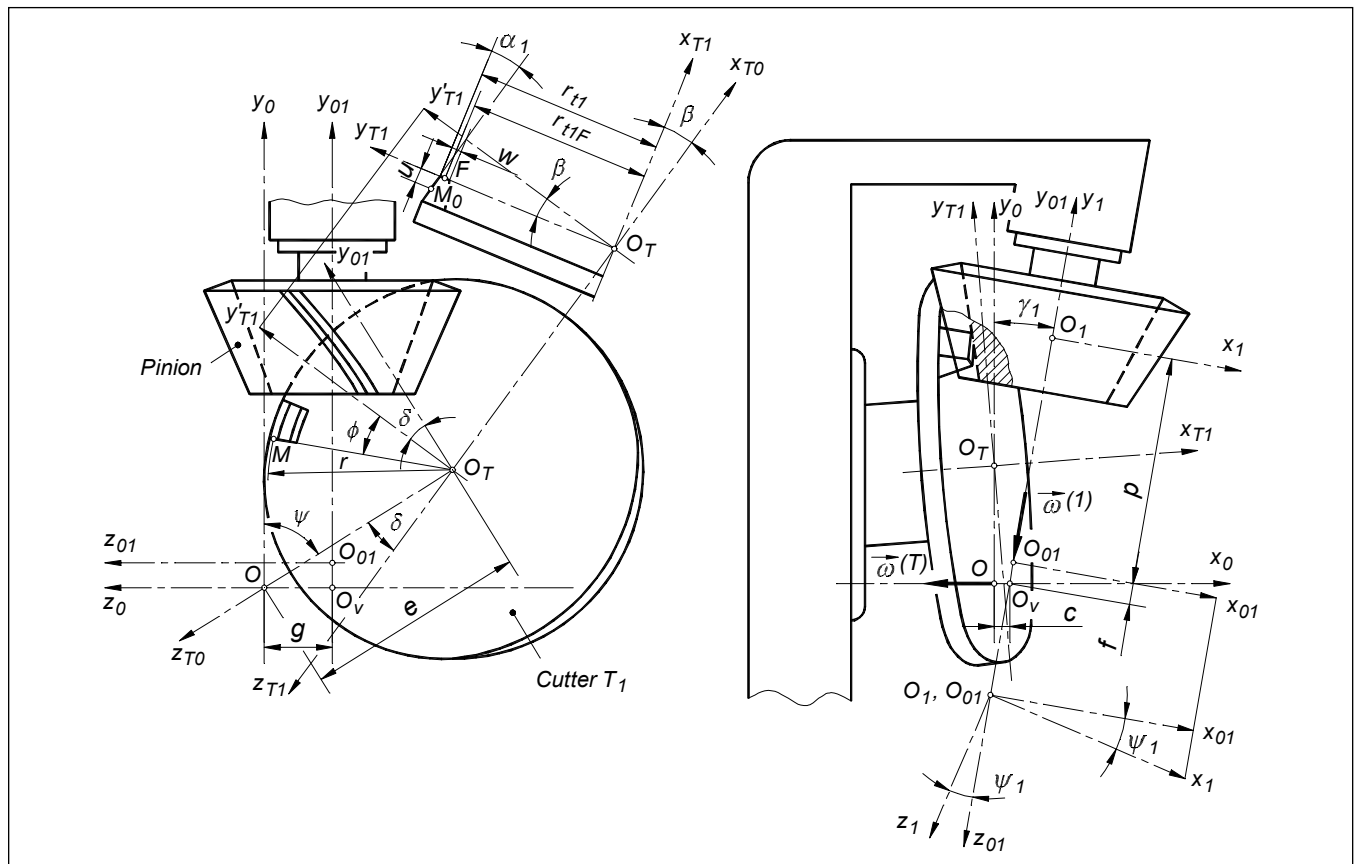


Figure 2—Machine tool setting for pinion tooth finishing.

$$\vec{r}_{01} = M_{p3} \cdot \vec{r}_0 = \begin{bmatrix} \cos \gamma_1 & -\sin \gamma_1 & 0 & -c \cdot \cos \gamma_1 \\ \sin \gamma_1 & \cos \gamma_1 & 0 & -f - c \cdot \sin \gamma_1 \\ 0 & 0 & 1 & g \\ 0 & 0 & 0 & 1 \end{bmatrix} \cdot \vec{r}_0 \quad (9)$$

$$\vec{r}_1 = M_{p4} \cdot \vec{r}_{01} = \begin{bmatrix} \cos \psi_1 & 0 & \sin \psi_1 & 0 \\ 0 & 1 & 0 & -p \\ -\sin \psi_1 & 0 & \cos \psi_1 & 0 \\ 0 & 0 & 0 & 1 \end{bmatrix} \cdot \vec{r}_{01} \quad (10)$$

The surface of the tool used for gear tooth processing is in the coordinate system K_{T2} (attached to tool T_2), defined by the equation (Fig. 3.):

$$\vec{r}_{T2}^{(T2)}(t, \xi) = \begin{bmatrix} -t \\ (r_{t2} + t \cdot \operatorname{tg} \alpha_2) \cdot \cos \xi \\ (r_{t2} + t \cdot \operatorname{tg} \alpha_2) \cdot \sin \xi \\ 1 \end{bmatrix} \quad (11)$$

The position vector of the formed gear tooth surface points is obtained by simple coordinate transformation of vector (Eq. 11) from system K_{T2} into the system K_2 (attached to the gear), as follows:

$$\vec{r}_2^{(2)} = M_{g1} \cdot \vec{r}_{T2}^{(T2)} \quad (12)$$

The matrix of this coordinate transformation is given by the expression (Fig. 3):

$$M_{g1} = \begin{bmatrix} \sin \gamma_2 & -\cos \gamma_2 & 0 & d - h \cdot \cos \gamma_2 \\ \cos \gamma_2 & \sin \gamma_2 & 0 & h \cdot \sin \gamma_2 \\ 0 & 0 & 1 & -v \\ 0 & 0 & 0 & 1 \end{bmatrix} \quad (13)$$

The Generation of Tooth Surfaces in Hobbed Hypoid Gears

In this paper the face hobbing process is based on the generalized concept of hypoid gear generation in which the mating pinion and gear can be considered respectively, generated by the imaginary generating crown gear shown in Figure 4. This imaginary generating gear is a virtual gear whose teeth are formed by the traces of the cutting edges of the head cutter blades (Fig. 5), although its tooth number is not necessarily an integer. Rather, it can be considered as a special case of a hypoid gear with a 90° pitch angle.

In the face hobbing process, two independent motions—timed continuous indexing and generating motion—are superimposed. The indexing motion between the tool and the imaginary generating gear forms the tooth surface of the generating gear with the extended epicycloid lengthwise tooth curve (Fig. 4). The indexing relationship can be expressed as:

$$\frac{\omega^{(t)}}{\omega^{(c)}} = \frac{N_c}{N_b} = i_c \quad (14)$$

where: $\omega^{(t)}$ and $\omega^{(c)}$ denote the angular velocities of the head cutter and the imaginary generating gear N_b and N_c , the number of the head cutter's blade groups, and the number of

teeth of the imaginary generating gear, respectively.

The second related motion is the rolling motion of the generating gear and the rotation of the workpiece-generated gear (Fig. 4). It can be represented as:

$$\frac{\omega^{(w)}}{\omega^{(c)}} = \frac{N_c}{N_w} = i_g \quad (15)$$

continued

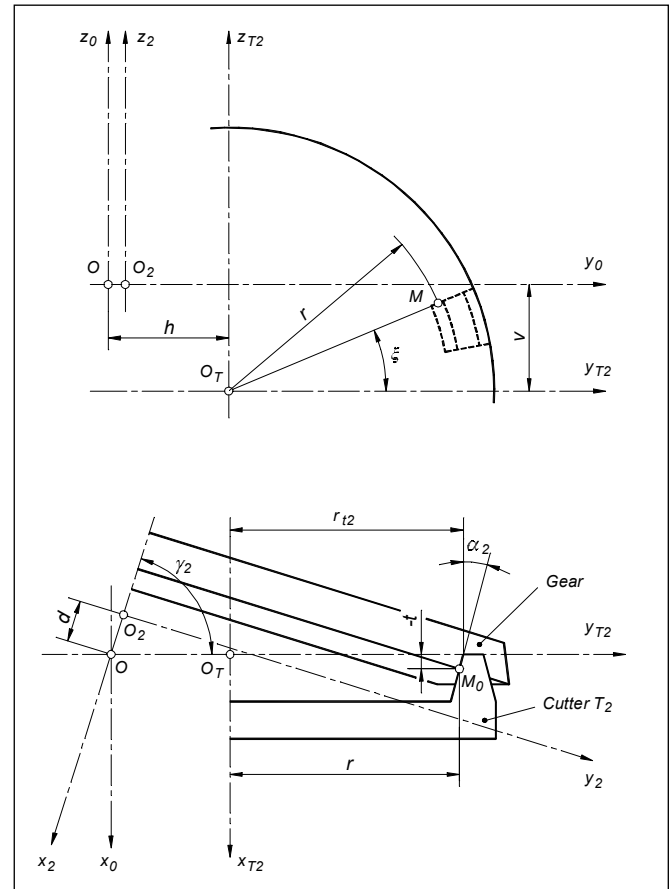


Figure 3—Machine tool setting for gear tooth finishing.

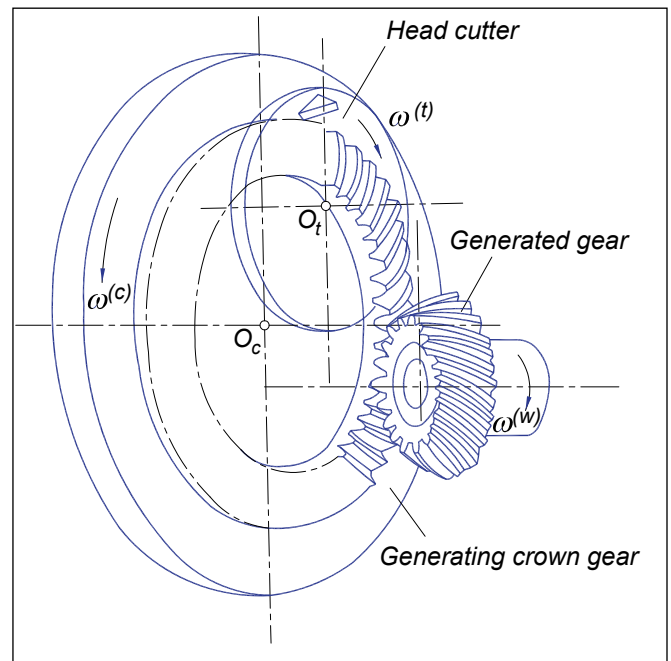


Figure 4—Concept of hypoid gear hobbing.

where: $\omega^{(w)}$ and N_w denote the angular velocity of the workpiece and the tooth number of the workpiece, respectively; and i_g is the ratio of roll in the generation of pinion and gear tooth surfaces.

Figure 5 shows the relative position between the head cutter and the imaginary generating crown gear. The relative position for two face hobbing methods for the implementation of the longitudinal tooth crowning of tooth flanks is presented:

- In the first system, two separate rotation centers with non-tilting cutter head cutter is applied to achieve lengthwise crowning.
- In the second method, cutter tilt is used to modify the curvatures of tooth surfaces.

In the generation process of the imaginary crown gear, the head cutter is rolling with its roll circle of radius ρ_t on the base circle of the imaginary crown gear of radius ρ_c without slippage. This rolling is realized by the rotations of the head cutter with angular velocity $\omega^{(t)}$ and of the crown gear with angular velocity $\omega^{(c)}$ around their axes in different directions (Fig. 5). The radii of rolling circles of the head cutter and of the generating crown gear are determined, respectively, by:

$$\rho_t = \frac{N_b}{N_b + N_c} \cdot e \quad (16)$$

$$\rho_c = \frac{N_c}{N_b + N_c} \cdot e \quad (17)$$

where: e is the radial machine setting.

In the system with non-tilting head cutter, the axes of the imaginary generating crown gear and of the head cutter are parallel. In the hypoid gear pair, where the convex gear flank rolls with the concave pinion flank, these are the “drive sides.” The other pair of flanks is the “coast side.” In Figure 5, the inside blade generates the convex gear tooth flank and the outer blade generates the concave pinion tooth flank. The lengthwise curvature of the concave surface is modified by increasing the radius of the outer head cutter. In addition, the eccentricity Δ and orientation angle $\Delta\psi$ of the outer rotation center O_{i0} to inner rotation center O_{ii} are used to control tooth thickness and contact position. The inside and outer blades are rigidly connected to the rolling circles with centers O_{ii} and O_{i0} , respectively. The effective cutting direction of the blades in the head cutter is not perpendicular to the cutter radius vector. The blades are moved in the head cutter tangentially to an offset position to accommodate the correct orientation with respect to the cutting motion vector. Therefore, the normal to the loci of blades at the middle point of tooth profiles, M_0 , has to pass through instantaneous centers of rotation O_i and O_o simultaneously. The profile of blades in the plane (y_e, z_e) of coordinate system $K_e(x_e, y_e \text{ and } z_e)$ may be a straight-lined or a circular arc in order to introduce tooth profile modification (Fig. 6).

Equation of the straight lined profile (based on Fig. 6a):

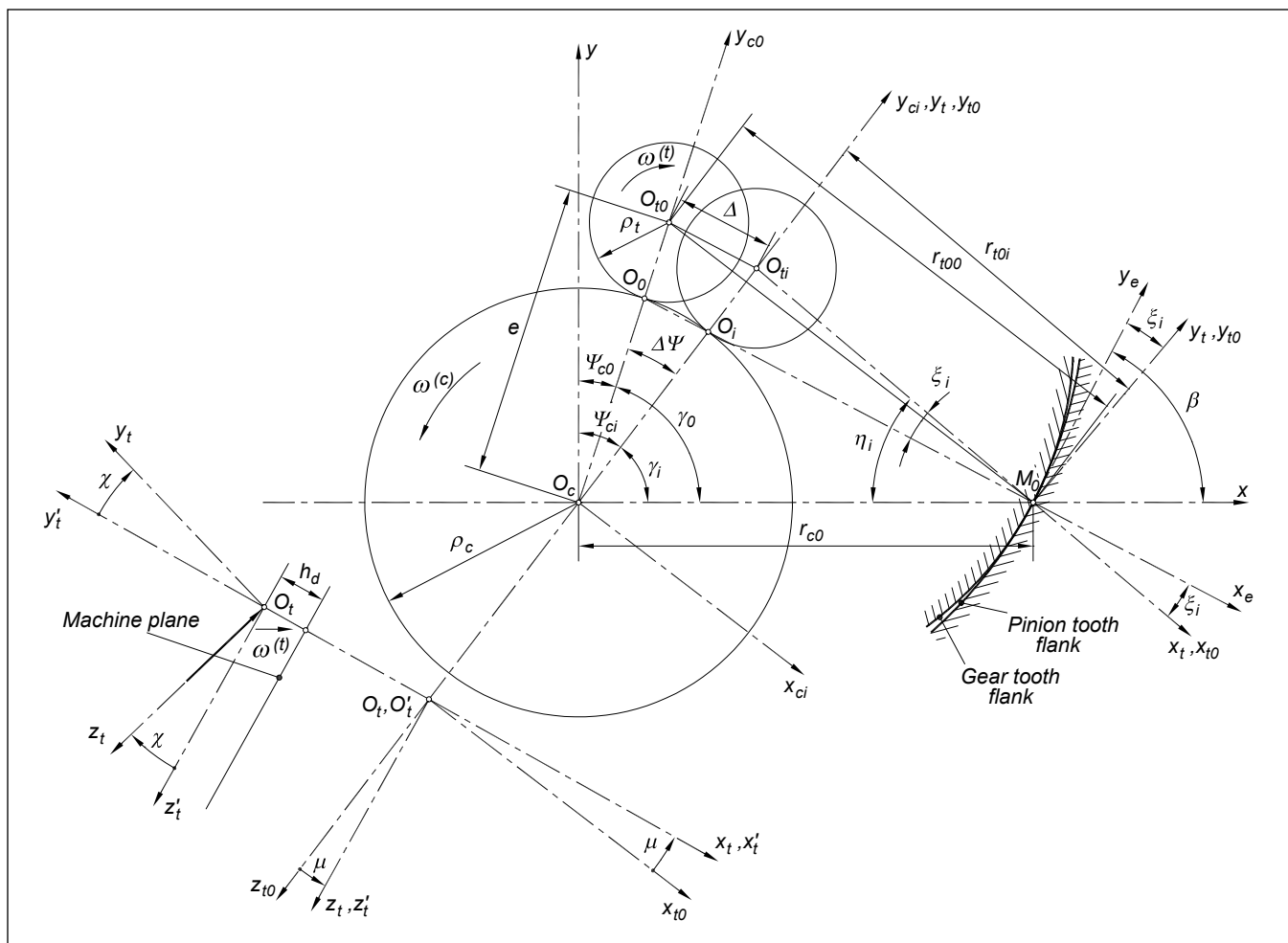


Figure 5—Relative position between the head cutter and the imaginary generating crown gear.

$$\vec{r}_e^{(e)}(u) = \begin{bmatrix} \text{sign} \cdot \left(\frac{s}{2} + u \cdot \text{tg} \alpha \right) \\ 0 \\ u \\ 1 \end{bmatrix} \quad (18)$$

Equation of the circular arc profile (based on Fig. 6b):

$$\vec{r}_e^{(e)}(v) = \begin{bmatrix} \text{sign} \cdot (x_{epi} + r_{profi} \cdot \cos v) \\ 0 \\ z_{epi} - r_{profi} \cdot \sin v \\ 1 \end{bmatrix} \quad (19)$$

where: $\text{sign} = 1$ for the convex tooth flank of the pinion and concave tooth flank of the gear; and $\text{sign} = -1$ for the concave tooth flank of the pinion and convex tooth flank of the gear member.

The tooth surface of the imaginary generating crown gear produced by coordinate transformation from coordinate system $K_e(x_e, y_e$ and $z_e)$ —rigidly connected to the head cutter—to coordinate system $K_c(x_c, y_c$ and $z_c)$ —connected to the imaginary generating crown gear—is represented by the following matrix equation (Figs. 5 and 7):

$$\vec{r}_c = \mathbf{M}_{c4} \cdot \mathbf{M}_{c3} \cdot \mathbf{M}_{c2} \cdot \mathbf{M}_{c1} \cdot \vec{r}_e = \mathbf{M}_{ec} \cdot \vec{r}_e \quad (20)$$

The coordinate transformations between the main coordinate systems $K_e(x_e, y_e$ and $z_e)$, $K_c(x_c, y_c$ and $z_c)$ and the auxiliary coordinate systems (Figs. 5 and 7), are performed as follows:

$$\vec{r}_t = \mathbf{M}_{c1} \cdot \vec{r}_e^{(e)} = \begin{bmatrix} \cos \xi_i & -\sin \xi_i & 0 & r_{t0} \\ \sin \xi_i & \cos \xi_i & 0 & 0 \\ 0 & 0 & 1 & 0 \\ 0 & 0 & 0 & 1 \end{bmatrix} \cdot \vec{r}_e^{(e)} \quad (21)$$

$$\vec{r}_{t0} = \mathbf{M}_{c2} \cdot \vec{r}_t = \begin{bmatrix} \cos \mu & -\sin \mu \cdot \sin \kappa & \sin \mu \cdot \cos \kappa & 0 \\ 0 & \cos \kappa & \sin \kappa & h_d \\ -\sin \mu & -\cos \mu \cdot \sin \kappa & \cos \mu \cdot \cos \kappa & 0 \\ 0 & 0 & 0 & 1 \end{bmatrix} \cdot \vec{r}_t \quad (22)$$

$$\vec{r} = \mathbf{M}_{c3} \cdot \vec{r}_{t0} = \begin{bmatrix} \cos(\eta_i + \psi_i) & \sin(\eta_i + \psi_i) & 0 & e \cdot \cos \gamma_i \\ -\sin(\eta_i + \psi_i) & \cos(\eta_i + \psi_i) & 0 & e \cdot \sin \gamma_i \\ 0 & 0 & 1 & 0 \\ 0 & 0 & 0 & 1 \end{bmatrix} \cdot \vec{r}_{t0} \quad (23)$$

$$\vec{r}_c = \mathbf{M}_{c4} \cdot \vec{r} = \begin{bmatrix} \cos \psi_c & \sin \psi_c & 0 & 0 \\ -\sin \psi_c & \cos \psi_c & 0 & 0 \\ 0 & 0 & 1 & 0 \\ 0 & 0 & 0 & 1 \end{bmatrix} \cdot \vec{r} \quad (24)$$

In the case of non-tilting head cutter:

$$\vec{r}_{t0} = \mathbf{M}_{c2} \cdot \vec{r}_t = \begin{bmatrix} 1 & 0 & 0 & 0 \\ 0 & 1 & 0 & h_d \\ 0 & 0 & 1 & 0 \\ 0 & 0 & 0 & 1 \end{bmatrix} \cdot \vec{r}_t \quad (25)$$

Due to the indexing motion: $\psi_t = i_c \cdot (\psi_c - \psi_{c0})$; where: $\psi_c = -(90^\circ - \gamma_1)$, or $\psi_{c0} = -(90^\circ - \gamma_0)$.

To obtain the pinion/gear tooth surface in the generating process, the work gear is rolled with the imaginary crown gear. Figure 8 describes the coordinate systems between the imaginary generating crown gear and the work gears:

- Coordinate system $K_c(x_c, y_c$ and $z_c)$ is rigidly connected to the generating crown gear;
- Coordinate systems $K_1(x_1, y_1$ and $z_1)$ and $K_2(x_2, y_2$ and $z_2)$ are rigidly connected to the pinion and the gear, respectively.

continued

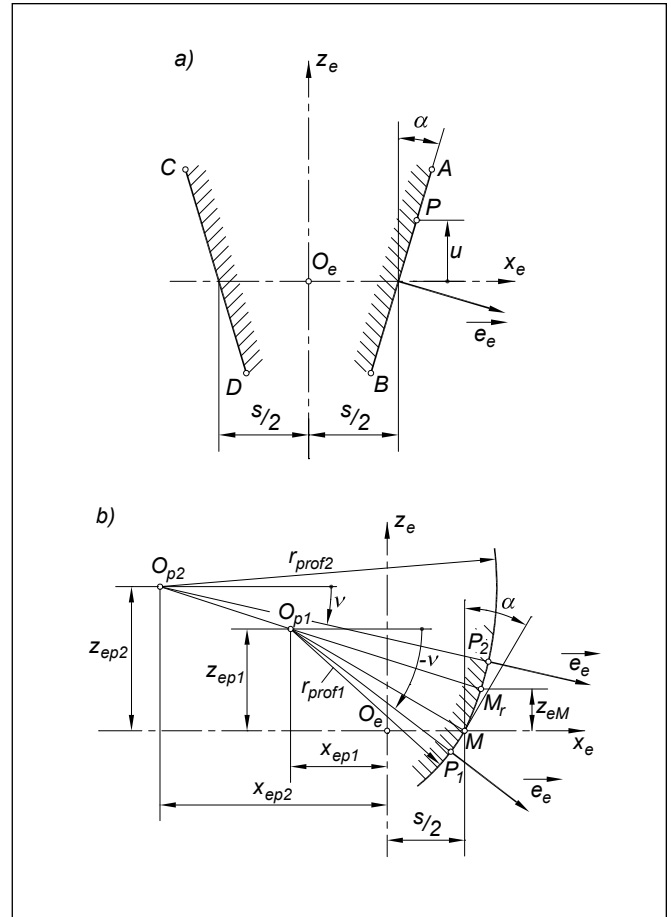


Figure 6—Blade profiles.

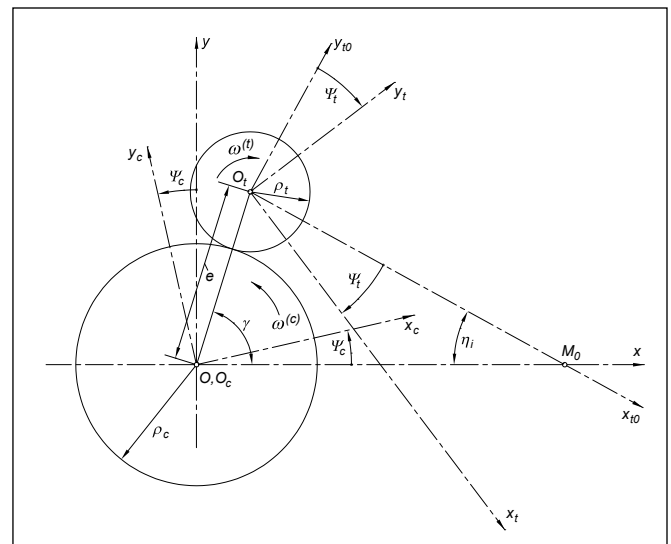


Figure 7—Rolling of head cutter and imaginary generating crown gear.

The tooth surfaces of the pinion and gear are defined by the following system of equations:

$$\vec{r}_i^{(i)} = \mathbf{M}_{i3} \cdot \mathbf{M}_{i2} \cdot \mathbf{M}_{i1} \cdot \vec{r}_c^{(i)} = \mathbf{M}_{i3} \cdot \mathbf{M}_{i2} \cdot \mathbf{M}_{i1} \cdot \mathbf{M}_{ec} \cdot \vec{r}_e^{(i)} \quad (26a)$$

$$\vec{v}_{c0}^{(c,i)} \cdot \vec{e}_{c0}^{(i)} = 0 \quad (26b)$$

The coordinate transformations between the main coordinate systems $K_c(x_c, y_c, z_c)$, $K_1(x_1, y_1, z_1)$, $K_2(x_2, y_2, z_2)$ and the auxiliary coordinate systems (Fig. 8), are performed as follows:

$$\vec{r}_{c0}^{(i)} = \mathbf{M}_{i1} \cdot \vec{r}_c^{(i)} = \begin{bmatrix} \cos \psi_{ci} & -\sin \psi_{ci} & 0 & 0 \\ \sin \psi_{ci} & \cos \psi_{ci} & 0 & 0 \\ 0 & 0 & 1 & 0 \\ 0 & 0 & 0 & 1 \end{bmatrix} \cdot \vec{r}_c^{(i)} \quad (27)$$

$$\vec{r}_{i0}^{(i)} = \mathbf{M}_{i2} \cdot \vec{r}_{c0}^{(i)} = \begin{bmatrix} -\sin \gamma_i & 0 & \cos \gamma_i & -c_i \cdot \cos \gamma_i \\ \cos \gamma_i & 0 & \sin \gamma_i & -c_i \cdot \sin \gamma_i - f_i \\ 0 & 1 & 0 & g_i \\ 0 & 0 & 0 & 1 \end{bmatrix} \cdot \vec{r}_{c0}^{(i)} \quad (28)$$

$$\vec{r}_i^{(i)} = \mathbf{M}_{i3} \cdot \vec{r}_{i0}^{(i)} = \begin{bmatrix} \cos \psi_i & 0 & \sin \psi_i & 0 \\ 0 & 1 & 0 & 0 \\ -\sin \psi_i & 0 & \cos \psi_i & 0 \\ 0 & 0 & 0 & 1 \end{bmatrix} \cdot \vec{r}_{i0}^{(i)} \quad (29)$$

$$\vec{v}_{c0}^{(c,i)} = \omega^{(c)} \cdot \begin{bmatrix} y_{c0}^{(i)} - i_{gi} \cdot (y_{c0}^{(i)} + g_i) \cdot \sin \gamma_i \\ -x_{c0}^{(i)} + i_{gi} \cdot [x_{c0}^{(i)} \cdot \sin \gamma_i - (z_{c0}^{(i)} - c_i) \cdot \cos \gamma_i] \\ i_{gi} \cdot (y_{c0}^{(i)} + g_i) \cdot \cos \gamma_i \end{bmatrix} \quad (30)$$

where: the velocity ratio in the kinematic scheme of the machine tool for the generation of pinion and gear tooth surfaces is:

$$i_{gi} = \frac{\omega^{(i)}}{\omega^{(c)}} = \frac{N_c}{N_i} \quad (31)$$

The normal surface vector of the imaginary generating crown gear for pinion and gear tooth-surface generation is:

$$\vec{e}_{c0}^{(i)} = \mathbf{M}_{i1} \cdot \vec{e}_c^{(i)} = \mathbf{M}_{i1} \cdot \mathbf{M}_{ec} \cdot \vec{e}_e^{(i)} \quad (32)$$

Loaded Tooth Contact Analysis

In order to determine maximum tooth contact pressure and transmission error, the new method of load distribution calculation is applied (Ref. 22).

The load distribution calculation is based on the conditions that the total angular position errors of the gear teeth being instantaneously in contact under load must be the same, and along the contact line (contact area) of every tooth pair instantaneously in contact, the composite displacements of tooth-surface points—as the sums of tooth deformations, tooth surface separations, misalignments, and composite tooth error— should correspond to the angular position of the gear member. Therefore, in all the points of the instantaneous contact lines, the following displacement compatibility equation should be satisfied:

$$\Delta \phi_2 = \Delta \phi_2^{(d)} + \Delta \phi_2^{(k)} = \frac{\Delta y_n}{r_D} \cdot \frac{|(\vec{r} \times \vec{a}_0) \cdot \vec{e}|}{|\vec{r}|} + \Delta \phi_2^{(k)} \quad (33)$$

where: Δy_n is the composite displacement of contacting surfaces in the direction of the unit tooth surface normal \vec{e} , \vec{r} is the position vector of the contact point, r_D is the distance of the contact point to the gear axis, and \vec{a}_0 is the unit vector of the gear axis.

The composite displacement of the contacting surfaces in contact point D, in the direction of the tooth-surface normal, can be expressed as:

$$\Delta y_n = w(z_D) + s(z_D) + e_n(z_D) \quad (34)$$

where: z_D is the coordinate of point D along the contact line, $w(z_D)$ is the total deflection in point D, $s(z_D)$ is the relative geometrical separation of tooth-surfaces in point D, and $e_n(z_D)$ is the composite error in point D, which is the sum of manufacturing and alignment errors of pinion and gear.

The total deflection in point D is defined by the following equation:

$$w(z_D) = \int_{L_{it}} K_d(z_D, z_F) \cdot p(z_F) \cdot dz + K_c(z_D) \cdot p(z_D) \quad (35)$$

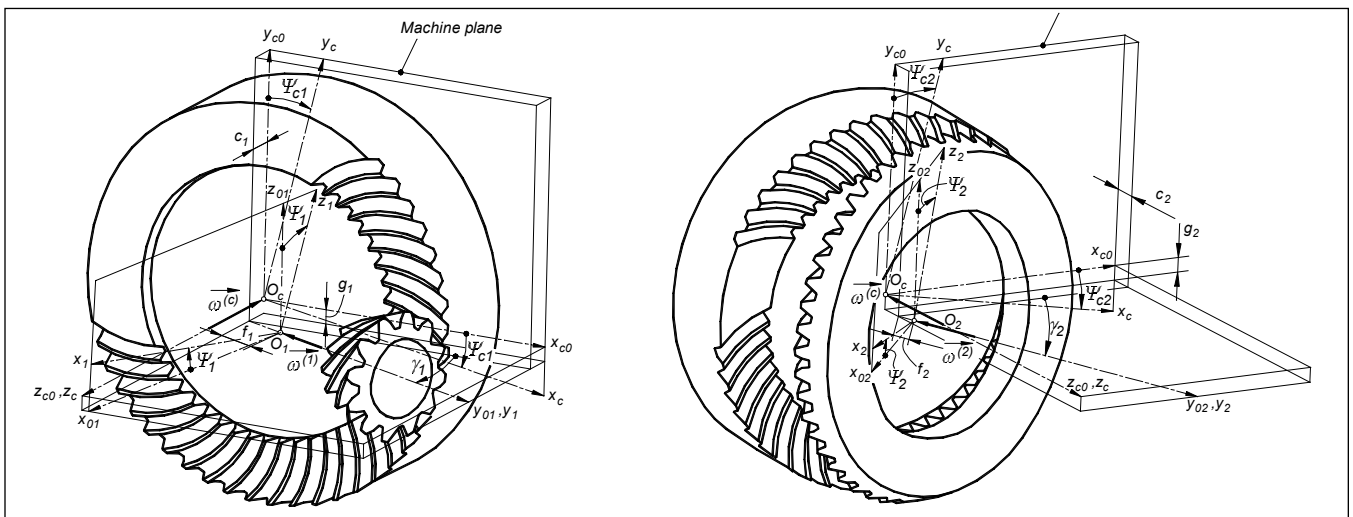


Figure 8—Generation of pinion and gear tooth surfaces.

where: L_{ii} is the geometrical length of the line of contact on tooth pair i , $K_d(z_D, z_F)$ is the influence factor of tooth load acting in tooth-surface point F on total composite deflection of pinion and gear teeth in contact point D. K_d includes the bending and shearing deflections of pinion and gear teeth, pinion and gear body bending and torsion, and deflections of supporting shafts. A finite element computer program is developed for the calculation of bending and shearing deflections in the pinion and in the gear. $K_c(z_D)$ is the influence factor for the contact approach between contacting pinion and gear teeth—i.e., the composite contact deformation in point D under load acting in the same point, and $p(z_F), p(z_D)$ are the tooth loads acting in positions F and D, respectively.

As the contact points are at different distances from the pinion/gear axis, the transmitted torque is defined by the equation:

$$T = \sum_{i=1}^{i=N_i} \int_{L_{ii}} r_F \cdot |\vec{p}(z_F) \cdot \vec{t}_{0F}| \cdot dz \quad (36)$$

where: r_F is the distance of the loaded point F to the gear axis, \vec{t}_{0F} is the tangent unit vector to the circle of radius r_F , passing through the loaded point F in the transverse plane of the gear, and N_i is the number of gear tooth pairs instantaneously in contact.

The load distribution on each line of contact can be calculated by solving the nonlinear system of Equations 33–36. An approximate and iterative technique is used to attain the solution. The contact lines are discretized into a suitable number of small segments, and the tooth contact pressure, acting along a segment, is approximated by a concentrated load, ΔF , acting in the midpoint of the segment. The actual load distribution, defined by the values of load ΔF , is obtained by using the “successive-over-relaxation method.” In every iteration cycle, a search for the points of the “potential” contact lines that could be in instantaneous contact is performed. For these points, the following condition should be satisfied:

$$\Delta y_{n(i_i, i_z)} \leq \frac{\Delta \phi_2 - \Delta \phi_{2(i_i)}^{(k)}}{\left(\frac{|\vec{r} \times \vec{a}_0 \cdot \vec{e}|}{r_D \cdot |\vec{r}|} \right)_{(i_i, i_z)}} \quad (37)$$

The details of the method for load distribution calculation in hypoid gears are described in Reference 22.

Transmission Error

Total transmission error consists of kinematical transmission error due to a mismatch of the gear pair, eventual tooth errors, misalignment of the meshing members and transmission error caused by tooth deflection.

It is assumed that the pinion is the driving member and is rotating at a constant velocity. As the result of the gears mismatch, a varying, angular velocity ratio of the gear pair—and an angular displacement of the gear member from the theoretically exact position based on the ratio of the number of teeth—occur. This angular displacement of the gear can be expressed as:

$$\Delta \phi_2^{(k)} = \phi_2 - \phi_{20} - N_1 \cdot (\phi_1 - \phi_{10}) / N_2 + \Delta \phi_{2s} \quad (38)$$

where:

- ϕ_{10} and ϕ_{20} are the initial angular positions of the pinion and the gear.

- ϕ_2 is the instantaneous angular position of the gear for a particular angular position of the pinion ϕ_1 .
- N_1 and N_2 are the numbers of pinion and gear teeth, respectively.
- $\Delta \phi_{2s}$ is the angular displacement of the gear due to edge contact misalignment of the mating members when a “negative” separation occurs on a tooth pair different from the tooth pair for which the angular position is calculated.

The angular displacement of the gear, $\Delta \phi_2^{(d)}$, caused by the variation of the compliance of contacting pinion and gear teeth rolling through mesh, is obtained as one of the results of the load distribution calculation. Therefore, the total angular position error of the gear is defined by the equation:

$$\Delta \phi_2 = \Delta \phi_2^{(k)} + \Delta \phi_2^{(d)} \quad (39)$$

Computed Results

The computer program, based on the theoretical background presented, has been applied for the investigation of the combined influence of machine tool settings; head cutter’s profile and diameter for pinion finishing; misalignments of the mating members on load distribution; maximum tooth contact pressure (p_{max}); and angular displacement of the driven gear member from the theoretically exact position based on the ratio of the number of teeth ($\Delta \phi_{2max}$). The calculation was carried out for the hypoid gear pair of design data given in Table 1.

The influence of machine settings; sliding base setting (c); basic machine center (f); basic offset setting (g); swivel angle (δ) (Fig. 2) on maximal tooth contact pressure (p_{max}); load distribution factor (β_F); and transmission error ($\Delta \phi_2$) is shown in Figs. 9–12. Factors $k_{p_{max}}$, k_{β_F} and $k_{\Delta \phi_2}$ represent the ratios of maximum tooth contact pressures, load distribution factors and transmission errors obtained by applying arbitrarily chosen values of machine tool setting parameters for pinion tooth generation and obtained by applying the basic values of these

continued

Table 1—Pinion and gear design data		
	Pinion	Gear
Number of teeth	11	41
Module, mm	4.41402	
Running offset, mm	25.4	
Outside diameter, mm	77.585	181.859
Face width, mm	31.911	27.762
Crown to crossing point, mm	86.998	30.671
Front crown to crossing point, mm	57.684	
Mean radius, mm	27.495	77.274
Mean spiral angle, deg	50.2597	32.3007
Pitch angle, deg	18.5400	70.5799
Face angle of blank, deg	23.2733	71.5859
Root angle, deg	17.5722	65.6684
Pitch apex beyond crossing point, mm		-0.023
Face apex beyond crossingpoint, mm	3.193	-0.398
Root apex beyond crossing point, mm	5.735	0.767
Mean addendum, mm		1.083
Mean dedendum, mm		6.295
Mean working depth, mm		6.372
Minimal normal topland width, mm		1.930

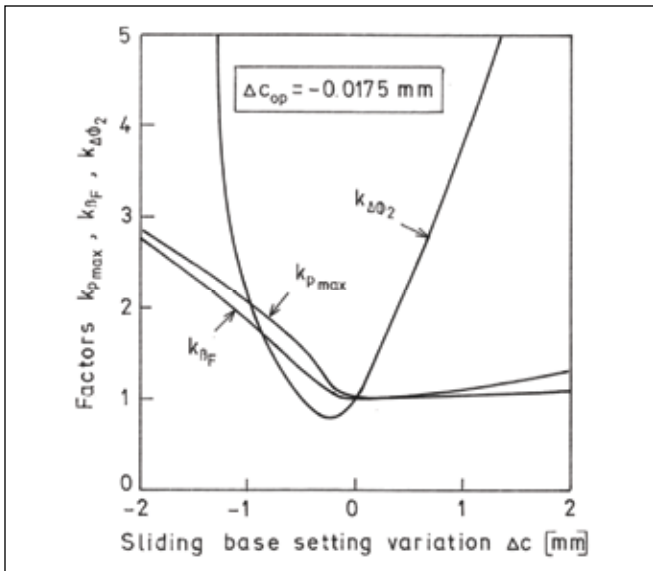


Figure 9—Influence of sliding-base-setting variation on load distribution and transmission error.

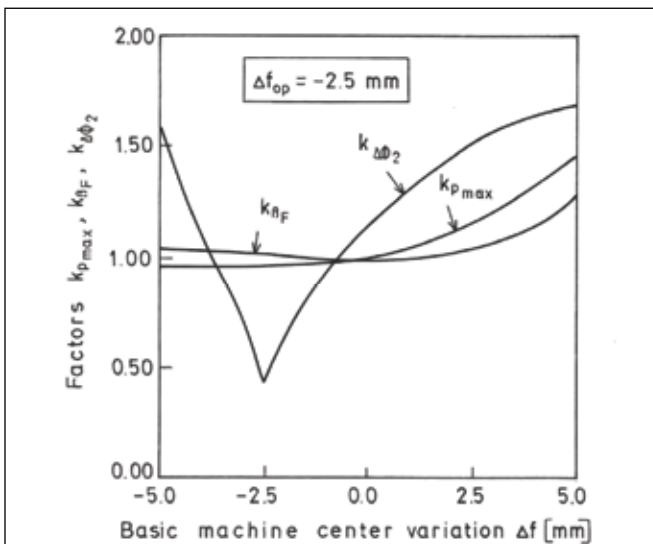


Figure 10—Influence of basic machine-center variation on load distribution and transmission error.

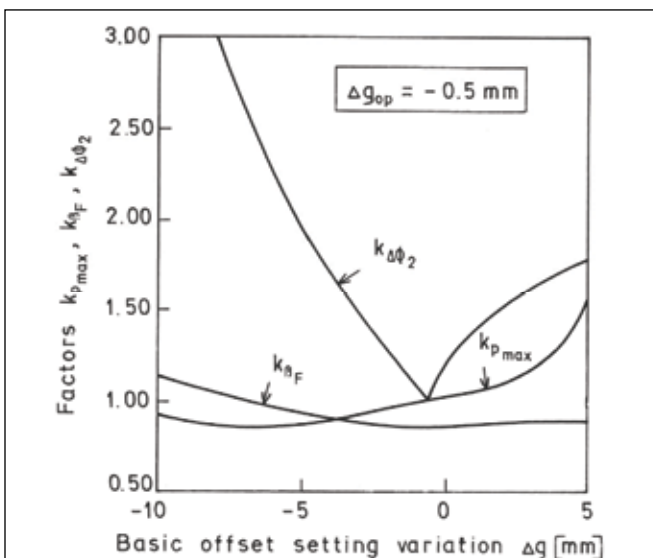


Figure 11—Influence of basic offset-setting variation on load distribution and transmission error.

parameters calculated by the Gleason or Litvin, et al., method (Refs. 41–42).

On the basis of obtained results, optimization of the machine tool setting was performed. By applying the optimized machine tool setting, the maximum tooth contact pressure was reduced by 5.8% and the angular position error of the driven gear by 65.4% when the pinion is finished by the machine tool setting determined by the commonly used methods.

The investigations have shown that a much better tooth contact pattern and less transmission error are obtained by finishing the pinion teeth with a cutter profile consisting of two circular arcs with radii of $r_{prof1} = 300$ mm, $r_{prof2} = -1,150$ mm (it means that the tool profile segment of radius r_{prof2} is convex), and when the cutter radius is corrected with $\Delta r_{H1} = -0.18$ mm. By applying these optimal values of cutter parameters, the maximum tooth contact pressure is reduced by 16% and the angular position error of the driven gear by 179%.

The influence of the angular misalignment of the pinion's shaft ε_v and the cutter's parameters on maximum tooth contact pressure was investigated. The computer simulation of loaded tooth contact analysis has shown that the influence of angular pinion shaft misalignment on the optimal value of profile radius r_{prof1} is negligible, but its effect on optimal profile radius r_{prof2} is considerable (Fig. 13). It can be noted that the optimal values of profile radius r_{prof2} are moved towards its higher values by the increase of angle ε_h (Fig. 13). The character of curves in Figure 14 indicates that angular shaft misalignment has little effect on optimal cutter radius correction.

Conclusions

A method is presented for the optimization of machine tool setting parameters and cutter for pinion finishing of face milled and face hobbled hypoid gear pairs. The aim of this optimization is to improve load distribution by reducing maximum tooth contact pressure and transmission error. On the basis of the obtained results the following conclusions are made:

- By applying the optimized machine tool setting, the maximum tooth contact pressure is reduced by 5.8%, the load distribution factor by 5.9%, and the angular position error of the driven gear by 65.4% when the pinion is finished by the machine tool setting determined by the commonly used methods.
- By applying the optimal cutter profile and diameter for pinion finishing, the maximum tooth contact pressure is reduced by 16% and the angular position error of the driven gear by 179%, when the hypoid gear pair is manufactured by cutter parameters determined by the commonly used methods. Also, by applying the optimal cutter parameters, the influence of shaft misalignments on maximum tooth contact pressure is reduced. ⚙️

Acknowledgments

The author would like to thank the Hungarian Scientific Research Fund (OTKA) for their financial support of the research under Contract Nos. K 62722 and K 77921.

References

1. Simon, V. "Optimal Tooth Modifications for Spur and He-

lical Gears,” *ASME Journal of Mechanisms, Transmissions and Automation in Design*, 111 (1989), 611–615.

2. Gonzalez-Perez, I., A. Fuentes, F. L. Litvin, K. Hayasaka and K. Yukishima. “Application and Investigation of Modified Helical Gears with Several Types of Geometry,” *Proceedings of the 10th ASME International Power Transmission and Gearing Conference*, Las Vegas, 2007, Paper No. DETC2007/PTG-34027, 1–10.

3. Lee, C.K. “Manufacturing Process for a Cylindrical Crown Gear Drive with a Controllable Fourth-Order Polynomial Function of Transmission Error,” *Journal of Material Processing Technology*, 209 (2009), 3–13.

4. Litvin, F.L. and Y. Zhang. “Local Synthesis and Tooth Contact Analysis of Face-Milled Spiral Bevel Gears,” NASA, CR-4342 (AVSCOM TR-90-C-028), 1991.

5. Argyris, J., A. Fuentes and F.L. Litvin. “Computerized Integrated Approach for Design and Stress Analysis of Spiral Bevel Gears,” *Computer Methods in Applied Mechanics and Engineering*, 191 (2002), 1057–1095.

6. Litvin, F.L. and A. Fuentes. *Gear Geometry and Applied Theory*, Cambridge University Press, Cambridge, 2004.

7. Lin, C.Y. and C.B. Tsay. “Mathematical Model of Spiral Bevel and Hypoid Gears Manufactured by the Modified Roll Method,” *Mechanism and Machine Theory*, 32 (1996), 121–136.

8. Stadtfeld, H.J. and U. Gaiser. “The Ultimate Motion Graph,” *ASME Journal of Mechanical Design*, 122 (2000), 317–322.

9. Wang, P.Y. and Y.H. Fong. “Fourth-Order Kinematic Synthesis for Face Milling Spiral Bevel Gears with Modified Radial Motion (MRM) Correction,” *ASME Journal of Mechanical Design*, 128 (2006), 457–467.

10. Di Puccio, F., M. Gabiccin and M. Guiggiani. “An Invariant Approach for Gear Generation with Supplemental Motions,” *Mechanism and Machine Theory*, 42 (2007), 275–295.

11. Artoni, A., A. Bracci, M. Gabaccini and M. Guiggiani. “Optimization of the Loaded Contact Pattern in Hypoid Gears by Automatic Topography Modification,” *ASME Journal of Mechanical Design*, 131 (2009), Art. No. 011008, 1–9.

12. Kawasaki, K., H. Tamura and Y. Iwamoto. “Klingelnberg Spiral Bevel Gears with Small Spiral Angles,” *Proceedings of the 4th World Congress on Gearing and Power Transmissions*, Paris, 1999, 697–703.

13. Stadtfeld, H. J. “The Basics of Gleason Face-Hobbing,” Gleason Works, 2000, 1–5.

14. Lelkes, M., J. Márialigeti and D. Play. “Numerical Determination of Cutting Parameters for the Control of Klingelnberg Spiral Bevel Gear Geometry,” *ASME Journal of Mechanical Design*, 124 (2002), 761–771.

15. Fan, Q. “Computerized Modeling and Simulation of Spiral Bevel and Hypoid Gears Manufactured by Gleason Face-Hobbing Process,” *ASME Journal of Mechanical Design*, 128 (2006), 1,315–1,327.

16. Fan, Q., R.S. DaFoe and J.W. Swanger. “Higher-Order Tooth Flank Form Error Correction for Face Milled Spiral Bevel and Hypoid Gears,” *ASME Journal of Mechanical Design*, 130 (2008), Art. No. 072601–7.

17. Shih, Y.P., Z.H. Fong and D.C.Y. Lin. “Mathematical Model for a Universal Face Hobbing Hypoid Gear Generator,”

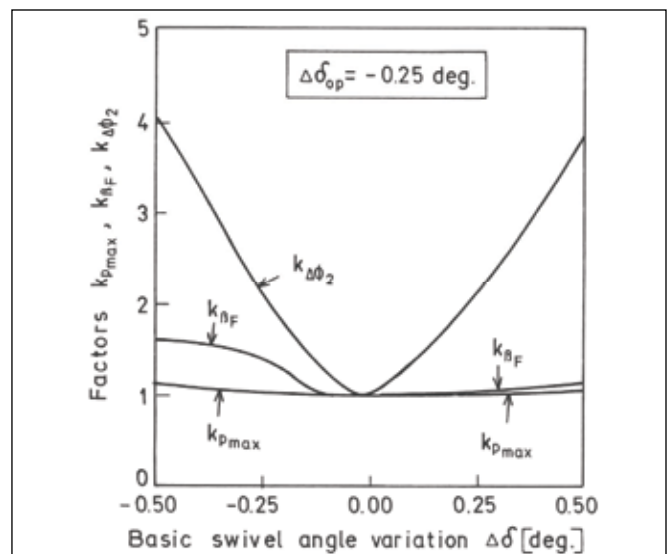


Figure 12—Influence of basic swivel-angle variation on load distribution and transmission error.

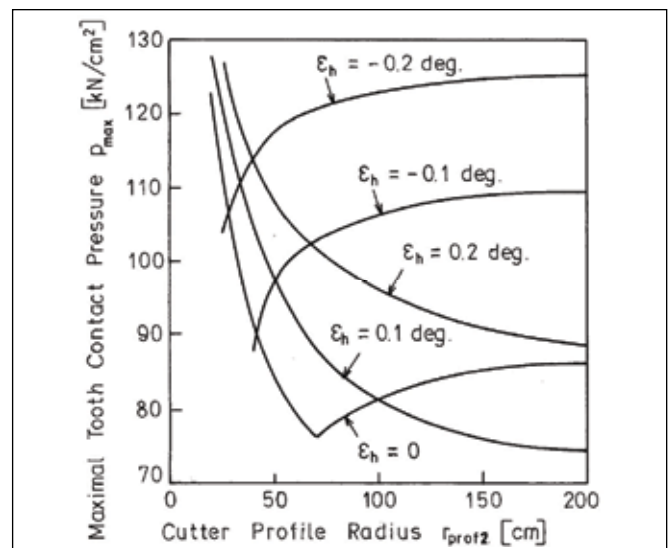


Figure 13—Influence of cutter-profile radius $r_{prof 2}$ and angular-shaft misalignment in the horizontal plane on maximal tooth contact pressure.

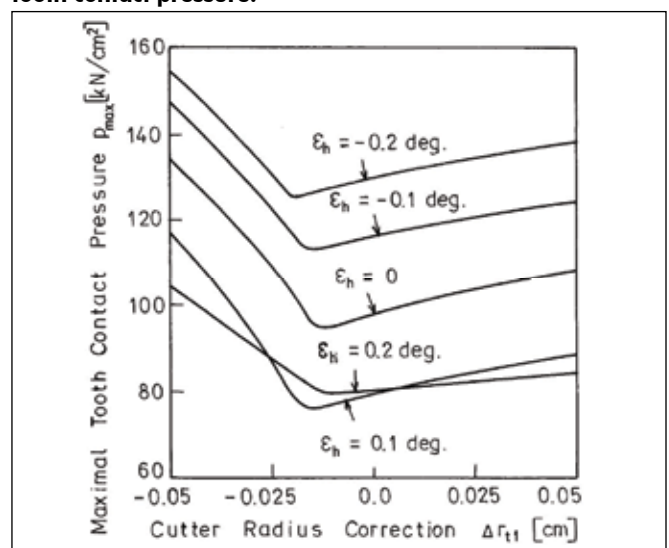


Figure 14—Influence of cutter radius correction and angular-shaft misalignment in the horizontal plane on maximal tooth contact pressure.

ASME Journal of Mechanical Design, 129 (2007), 38–47.

18. Shih, Y.P. and Z.H. Fong. “Flank Correction for Spiral Bevel and Hypoid Gears on a Six-Axis CNC Hypoid Generator,” *ASME Journal of Mechanical Design*, 130 (2008), Art. No. 062604, 1–11.

19. Vimercati, M. “Mathematical Model for Tooth Surfaces Representation of Face Hobbed Hypoid Gears and its Application to Contact Analysis and Stress Calculation,” *Mechanism and Machine Theory*, 42 (2007), 668–690.

20. Zhang, Y. and Z. Wu. “Geometry of Tooth Profile and Fillet of Face Hobbed Spiral Bevel Gears,” *Proceedings Of the 10th ASME International Power Transmission and Gearing Conference*, Las Vegas, 2007, Paper No. DETC2007/PTG-34123, 1–12.

21. Simon, V. “Tooth Contact Analysis of Mismatched Hypoid Gears,” *Proceedings of the 7th International Power Transmission and Gearing Conference*, San Diego 1996, 789–798.

22. Simon, V. “Load Distribution in Hypoid Gears,” *ASME Journal of Mechanical Design*, 122 (2000), 529–535.

23. Simon, V. “Optimal Tooth Modifications in Hypoid Gears,” *ASME Journal of Mechanical Design*, 127 (2005), 646–655.

24. Simon, V. “Optimal Tooth Modifications in Spiral Bevel Gears Introduced by Machine Tool Setting Variation,” *Proceedings of the AGMA Fall Technical Meeting*, Orlando 2006, Paper No. 06FTM15, 1–12.

25. Simon, V. “Computer Simulation of Tooth Contact Analysis of Mismatched Spiral Bevel Gears,” *Mechanism and Machine Theory*, 42 (2007), 365–381.

26. Simon, V. “Load Distribution in Spiral Bevel Gears,” *ASME Journal of Mechanical Design*, 129 (2007), 201–209.

27. Simon, V. “Design and Manufacture of Spiral Bevel Gears with Reduced Transmission Errors,” *ASME Journal of*

Mechanical Design, 131 (2009), Art. No. 041007, Pg. 1–11.

28. Bair, B.W and C.B. Chung. “Effects of Profile Shifted Factor and Pressure Angle on the ZK-Type Dual-Lead Worm Gear Drives,” *Materials Processing Technology*, 112 (2001), 29–36.

29. Liu, C.C., J.H. Chen, C.B. Tsay and Y. Ariga. “Meshing Simulations of the Worm Gear Cut by a Straight-Edged Flyblade and the ZK-Type Worm with a Non-90 Crossing Angle,” *Mechanism and Machine Theory*, 41 (2006), 987–1002.

30. Hiltcher, Y., M. Guingand and J.P. Vaujany. “Numerical Simulation and Optimization of Worm Gear Cutting,” *Mechanism and Machine Theory*, 41 (2006), 1090–1110.

31. Litvin, F.L., I. Gonzalez-Perez, K. Yukishima, A. Fuentes and K. Hayasaka. “Design, Simulation of Meshing and Contact Stresses for Improved Worm Gear Drive,” *Mechanism and Machine Theory*, 42 (2007), 940–959.

32. Litvin, F.L., K. Yukishima, K. Hayasaka, I. Gonzalez-Perez and A. Fuentes. “Geometry and Investigation of Klingelnberg-Type Worm Gear Drive,” *ASME Journal of Mechanical Design*, 129 (2007), 17–22.

33. Simon, V. “Characteristics of a New Type of Cylindrical Worm Gear Drive,” *ASME Journal of Mechanical Design*, 120 (1998), 139–146.

34. Simon, V. “Computer-Aided Loaded Tooth Contact Analysis in Cylindrical Worm Gears,” *ASME Journal of Mechanical Design*, 127 (2005), 973–981.

35. Simon, V. “The Influence of Gear Hobbing on Worm Gear Characteristics,” *ASME Journal of Manufacturing Science and Engineering*, 129 (2007), 919–925.

36. Shi, W., D. Qin and W. Xu. “Meshing Control of the Double-Enveloping Worm Gearing Under the Conditions of Existing Errors and Load,” *Mechanism and Machine Theory*, 39 (2004), 61–74.

37. Qin, D., W. Shi and W. Xu. “Loaded Contact Analysis and Mesh Control on Double-Enveloping Hourglass Worm Gearing,” *Proceedings of the 12th IFTOMM World Congress*, Besancon 2007, Paper No. Gt-592, 1–5.

38. Chen, K.Y. and C.B. Tsay. “Mathematical Model and Worm Wheel Tooth Working Surfaces of the TN-Type Hourglass Worm Gear Set,” *Mechanism and Machine Theory*, 2009 (in press).

39. Simon, V. “A New Type of Ground Double Enveloping Worm Gear Drive,” *Proceedings of the ASME 5th International Power Transmissions and Gearing Conference*, Chicago 1989, 281–288.

40. Simon, V. “Load Distribution in Double-Enveloping Worm Gears,” *ASME Journal of Mechanical Design*, 115 (1993), 496–501.

41. Litvin, F.L. and Y. Gutman. “Methods of Synthesis and Analysis for Hypoid Gear Drives of Formate and Helixform,” Parts 1–3, *ASME Journal of Mechanical Design*, 103 (1981), 83–113.

42. Litvin, F.L., Y. Zhang, M. Lundy and C. Heine. “Determination of Settings of a Tilted Head Cutter for Generation of Hypoid and Spiral Bevel Gears,” *ASME Journal of Mechanisms, Transmissions and Automation in Design*, 110 (1988), 495–500.

Vilmos Simon received his B.S.E. in 1963 from the University of Belgrade; mechanical engineering (engineer specialist) and technical doctorate degrees (machine design) in 1968 from the University of Budapest; and a doctor of science degree (machine design) in 1996 from the Hungarian Academy of Science. His work, research and faculty experience include stints at the Jugoalat tool factory, Novi Sad; University of Novi Sad/Faculty of Technology; Szent István University of Godollo; Budapest University of Technology and Economics; Rochester Institute of Technology; Gleason Works; University of Pennsylvania; Philadelphia Gear; Zhengzhou Research Institute; and Technical University of Budapest. Simon’s many areas of expertise include—but are not limited to—geometry, kinematics, dynamics, manufacture and elastohydrodynamic analysis of lubrication; finite element development; creation of more than 30 computer programs in support of the above, and more. Simon has headed up a number of research projects and is the author of more than 50 papers and 80 conference presentations.

